Reciprocal regulation of eNOS and caveolin-1 functions in endothelial cells

Zhenlong Chen[a], Suellen D. S. Oliveira[a], Adriana M. Zimnicka[b], Ying Jiang[a], Tiffany Sharma[b], Stone Chen[c], Orly Lazarov[d], Marcelo G. Bonini[e], Jacob M. Haus[f], and Richard D. Minshall[a,b,*]
Departments of [a]Anesthesiology, [b]Pharmacology, [d]Anatomy and Cell Biology, [e]Medicine, and [f]Kinesiology and Nutrition, University of Illinois at Chicago, Chicago, IL 60612; [c]Whitney M. Young Magnet High School, Chicago, IL 60607

ABSTRACT **We hypothesized that the maintenance of vascular homeostasis is critically dependent on the expression and reciprocal regulation of caveolin-1 (Cav-1) and endothelial nitric oxide synthase (eNOS) in endothelial cells (ECs). Skeletal muscle biopsies from subjects with type 2 diabetes showed 50% less Cav-1 and eNOS than those from lean healthy controls. The Cav-1:eNOS expression ratio was 200:1 in primary culture human ECs. Cav-1 small interfering RNA (siRNA) reduced eNOS protein and gene expression in association with a twofold increase in eNOS phosphorylation and nitrate production per molecule of eNOS, which was reversed in cells overexpressing Adv-Cav-1-GFP. Upon addition of the Ca^{2+} ionophore A23187 to activate eNOS, we observed eNOS Ser1177 phosphorylation, its translocation to β-catenin-positive cell–cell junctions, and increased colocalization of eNOS and Cav-1 within 5 min. We also observed Cav-1 S-nitrosylation and destabilization of Cav-1 oligomers in cells treated with A23187 as well as insulin or albumin, and this could be blocked by L-NAME, PP2, or eNOS siRNA. Finally, caveola-mediated endocytosis of albumin or insulin was reduced by Cav-1 or eNOS siRNA, and the effect of Cav-1 siRNA was rescued by Adv-Cav-1-GFP. Thus, Cav-1 stabilizes eNOS expression and regulates its activity, whereas eNOS-derived NO promotes caveola-mediated endocytosis.**

Monitoring Editor
Alpha Yap
University of Queensland

Received: Jan 19, 2017
Revised: Feb 12, 2018
Accepted: Mar 12, 2018

INTRODUCTION

Nitric oxide (NO) is a highly lipophilic, reactive, diffusible free radical gas with a short half-life in biological fluids (Thomas *et al.*, 2001; Dudzinski *et al.*, 2006). NO is generated by three NO synthase (NOS) isoforms, namely, neuronal NOS (nNOS; encoded by *nos1*), inducible NOS (iNOS; encoded by *nos2*), and endothelial NOS (eNOS; encoded by *nos3*) (Shen *et al.*, 1999; Sears *et al.*, 2003; Qian and Fulton, 2013). In vascular endothelium, eNOS is constitutively expressed and the NO produced can react via S-nitrosylation of thiol groups on nearby proteins, resulting in modulation of cellular processes such as protein trafficking, redox state, and cell cycle (Iwakiri, 2011). The activity of eNOS in endothelial cells (ECs) is enhanced by agonists such as acetylcholine (ACh), bradykinin, and histamine, which increase intracellular calcium (Ca^{2+}), whereas hemodynamic shear stress and hormones such as insulin and plasma albumin increase eNOS-derived NO production independent of changes in intracellular Ca^{2+} (Maniatis *et al.*, 2006; Lundberg *et al.*, 2015; Zhao *et al.*, 2015).

Reduced expression and dysregulation of eNOS resulting in decreased NO bioavailability (i.e., eNOS uncoupling) is associated with cardiovascular disease (CVD) (Qian and Fulton, 2013). Endothelial dysfunction, manifested as an attenuation of NO-mediated vasodilation, is associated with several conditions such as obesity, insulin resistance, and type 2 diabetes mellitus (T2DM) that are strongly linked to CVD (Frank *et al.*, 2003; Mahmoud *et al.*, 2016). Direct binding of eNOS to the scaffolding domain of caveolin-1 (Cav-1) is a well-accepted mechanism for inactivating eNOS (Bernatchez *et al.*, 2005; Chen *et al.*, 2012), and the absence of Cav-1 is thought to promote eNOS dysfunction associated with CVD (Ju *et al.*, 1997; Zhao *et al.*, 2002; Yue *et al.*, 2012; Bakhshi *et al.*, 2013; Mao *et al.*, 2014; Oliveira *et al.*, 2017).

This article was published online ahead of print in MBoC in Press (http://www.molbiolcell.org/cgi/doi/10.1091/mbc.E17-01-0049) on March 22, 2018.

*Address correspondence to: Richard D. Minshall (rminsh@uic.edu).

Abbreviations used: A23187, calcium ionophore; Cav-1, caveolin-1; CVD, cardiovascular disease; ECs, endothelial cells; eNOS, endothelial nitric oxide synthase; GFP, green fluorescent protein; HEK, human embryonic kidney; HUVEC, human umbilical vein endothelial cells; LHC, lean healthy control; L-NAME, L-N^G-nitroarginine methyl ester (hydrochloride); PM, plasma membrane; PP2, 4-amino-5-(4-chlorophenyl)-7-(*t*-butyl) pyrazolo [3, 4-*d*] pyrimidine; Src, Src family kinase; T2DM, type 2 diabetes mellitus; YFP, yellow fluorescent protein.

Caveolae are 50–100-nm-diameter cell surface plasma membrane invaginations that play key roles in endocytosis, transcytosis, lipid homeostasis, signal transduction, and mechanoprotection (for review, see Shvets *et al.*, 2014). Depletion of Cav-1 and resultant reduction in number of caveolae have recently been linked to a wide range of human disease states, including cardiovascular and pulmonary disease (Bakhshi *et al.*, 2013; Parton and del Pozo, 2013; Oliveira *et al.*, 2017). Cav-1 is the most abundant protein associated with caveolae and is required for caveola formation in nonmuscle cells (Parton and Simons, 2007; Pavlides *et al.*, 2014). In particular, Cav-1 is highly expressed in ECs (Frank *et al.*, 2003), and our group has shown that phosphorylation of Cav-1 Tyr14 by Src kinase is required for caveola-mediated endocytosis and trafficking (Shajahan *et al.*, 2004; Hu *et al.*, 2006, 2008; Sun *et al.*, 2009; Sverdlov *et al.*, 2009; Zimnicka *et al.*, 2016). Cav-1 is a 22-kDa integral membrane protein that forms homo- and heterooligomers with adjacent Cav-1 and Cav-2 molecules via interaction of adjacent oligomerization/scaffolding domains (aa 61 or 82–101) and C-terminal Cys156 residues (Monier *et al.*, 1996; Song *et al.*, 1997; Fernandez *et al.*, 2002; Bakhshi *et al.*, 2013; Cheng and Nichols, 2016; Zimnicka *et al.*, 2016). In ECs, eNOS localization on caveolae is dependent on irreversible posttranslational myristoylation of eNOS N-terminal Cys15 and Cys26 (Robinson and Michel, 1995; Dudzinski *et al.*, 2006). eNOS associated with caveolae is held inactive by its direct interaction with Cav-1 via caveolin scaffolding domain (CSD)–dependent binding (Shaul *et al.*, 1996; Bernatchez *et al.*, 2011). Interestingly, upon stimulation of caveola-mediated endocytosis in microvascular ECs and mouse lung vessels, eNOS-derived NO production increases in a manner dependent on dynamin-2, Gβγ, PI3K, and Akt signaling (Maniatis *et al.*, 2006; Sánchez *et al.*, 2008; Liu *et al.*, 2012). Similar observations were reported for insulin (Wang *et al.*, 2009). eNOS-derived NO production increases Src activity and subsequent phosphorylation of Cav-1 Tyr14, resulting in increased caveola trafficking (Zimnicka *et al.*, 2016). Thus, transient activation of eNOS-derived NO production and resultant Src signaling are associated with an increase in caveola-mediated endocytosis and also promote Cav-1/eNOS binding and inactivation of eNOS (Chen *et al.*, 2012). Prolonged exposure to NO leads to Cav-1 nitrosation, phosphorylation, ubiquitination, and degradation (Bakhshi *et al.*, 2013; Mao *et al.*, 2014), which we hypothesize lead to eNOS hyperactivation and uncoupling (Bonini *et al.*, 2014).

In this study, we noted reduced Cav-1 and eNOS expression in skeletal muscle capillary endothelial cells from subjects with T2DM. We then attempted to understand the mechanistic basis for endothelial dysfunction by characterizing the stoichiometry of Cav-1-dependent regulation of eNOS expression and activity, determined whether this was dependent on eNOS and/or Src-mediated post-translational modifications to Cav-1, and also assessed whether eNOS-derived NO regulates critical Cav-1 scaffolding and endocytosis functions in ECs.

RESULTS

eNOS and Cav-1 expression level were determined in skeletal muscle biopsies obtained from subjects with T2DM and lean healthy controls (LHCs). Western blot analysis of skeletal muscle needle biopsies from subjects with T2DM (n = 8; Figure 1A) showed that Cav-1 and eNOS protein expression were significantly reduced (on the average; normalized to actin loading control) by more than 50% compared with LHCs (n = 10; Figure 1B). Immunohistochemical staining suggested that Cav-1 and eNOS proteins in fresh-frozen tissue sections localized, as expected, to endothelial cells in capillaries lying between muscle bundles (unpublished data). These results are consistent with the idea that reduction in Cav-1 expression and the associated eNOS dysfunction may be critical determinants of the cardiovascular complications of T2DM (Mahmoud *et al.*, 2016).

Calcium-ionophore–induced eNOS phosphorylation, translocation to plasma membrane cell–cell junctions, and colocalization with Cav-1

eNOS activity is dependent on intracellular calcium. Stimulation of HUVEC monolayers for 5 min with the Ca^{2+} ionophore A23187 induced eNOS translocation to cell–cell junctions where it colocalized with β-catenin (yellow, white arrows in Figure 2A) in confocal images. In addition, pS1177-eNOS similarly appeared at cell–cell junctions in cells treated with A23187 in contrast to untreated cells (Figure 2B). We further assessed whether activated eNOS colocalizes with Cav-1 at cell–cell junctions. Consistent with previous findings (Orlichenko *et al.*, 2009; Sun *et al.*, 2009), Cav-1 colocalized in part with β-catenin under basal conditions (Figure 2C, top panel), whereas following stimulation with A23187, we observed increased eNOS staining at cell–cell junctions, which colocalized with both β-catenin and Cav-1 (Figure 2C). Normalized data showed that the relative amount of eNOS at junctions increased significantly by 40% (see region of interest [ROI]) compared with untreated cells (Figure 2D). These data suggest that after stimulation, phospho-eNOS accumulates at the membrane and cell–cell junctions, where it colocalizes with Cav-1.

NO/Src-dependent Cav-1 S-nitrosylation and dissociation of high-molecular-weight oligomers induced by A23187

Previously, we showed that tumor necrosis factor α (TNF-α) induces NO production and S-nitrosylation of Cav-1 Cys156 in human lung endothelial cells (Bakhshi *et al.*, 2013). Here, we tested whether NO generation in HUVEC promotes Cav-1 S-nitrosylation and whether this is associated with a change in Cav-1 oligomerization or caveolae-mediated endocytosis. Indeed, enhanced Cav-1 S-nitrosylation (2.4-fold) was observed upon stimulation with A23187 for 5 min. S-nitrosylation of Cav-1 was reduced significantly by L-NAME (Figure 3A) or when eNOS was depleted by small interfering RNA (siRNA) (Supplemental Figure 1), indicating that Cav-1 S-nitrosylation is eNOS/NO-dependent. Surprisingly, A23187-induced Cav-1 S-nitrosylation was also abolished in cells pretreated with PP2 (15 μM; Src kinase

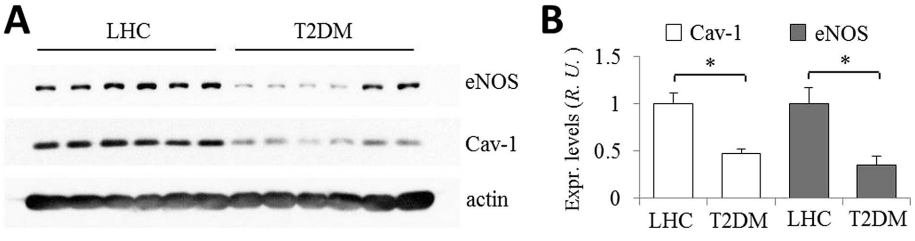

FIGURE 1: eNOS and Cav-1 expression level in human biopsies from LHC donors and patients with T2DM. (A) Skeletal muscle needle biopsies were obtained from LHC donors (n = 10) and subjects with T2DM (n = 8), homogenized in RIPA buffer, and assessed by Western blotting. A quantity of 30 μg total protein per sample was loaded per lane and the blots were probed for eNOS, Cav-1, and actin. (B) Normalized values of eNOS and Cav-1 expression in LHC donors (set as 1) were reduced by ~50% in patients with T2DM. *, $p < 0.01$.

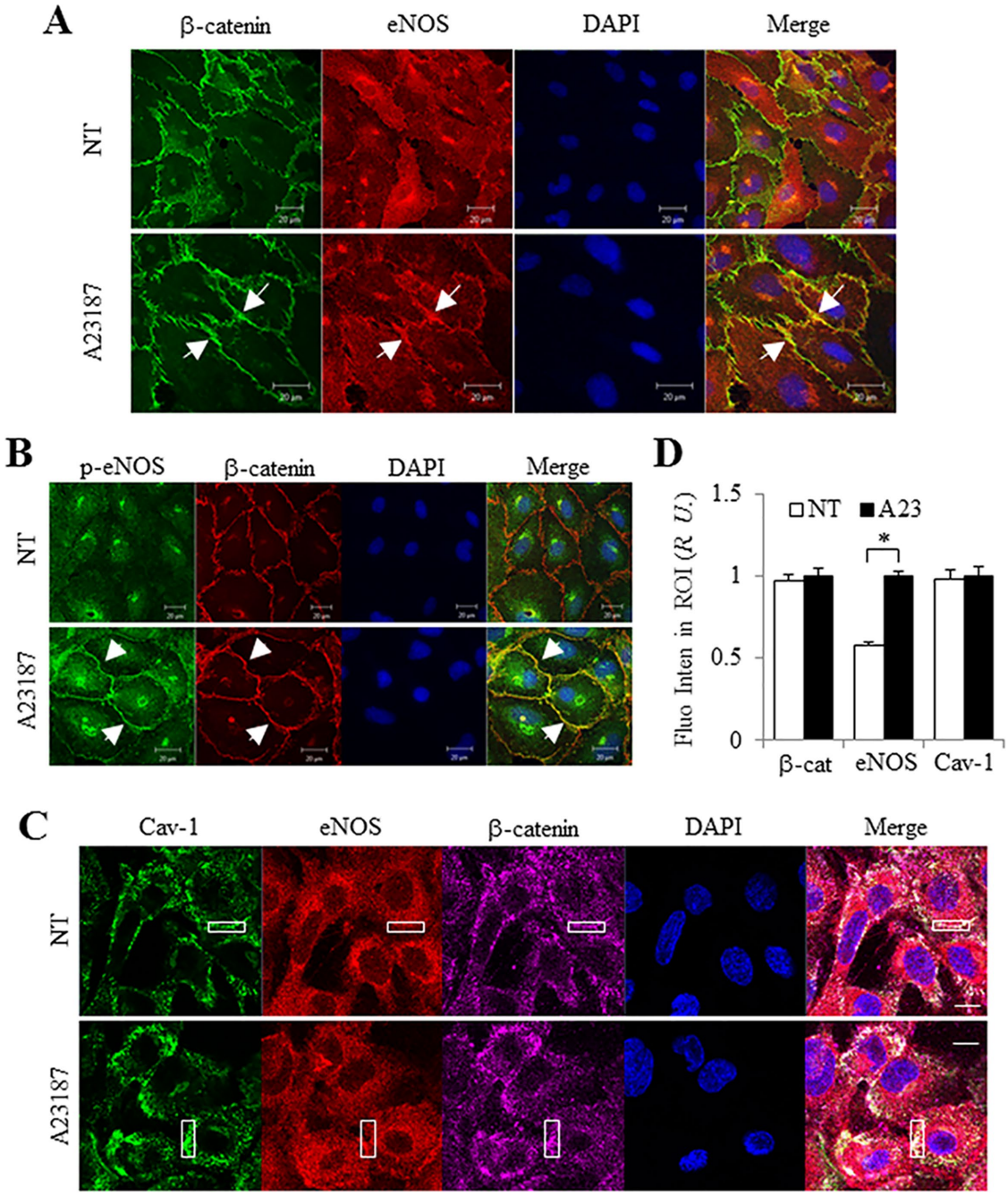

FIGURE 2: eNOS translocation to cell–cell junctions colocalizes with Cav-1. After stimulation with 5 μM A23187 for 5 min at 37°C, HUVECs were fixed and immunostained. (A) After activation, eNOS (red) translocated to cell–cell junctions (indicated by white arrow) as shown by β-catenin (green) staining in HUVECs. (B) Phospho-eNOS Ser1177 (green) colocalized (indicated by white arrow) with β-catenin (red), and (C) total eNOS (red) colocalized with Cav-1 (green) on cell–cell junctions (purple) after treatment with 5 μM A23187. Confocal images are representative of at least four independent experiments. DAPI was used to stain the nucleus. Scale bar, 20 μm. (D) Normalized fluorescence intensity in the region of interest (ROI, indicated as white box) was obtained using the histogram function of Zeiss Zen Blue software on the LSM 880 microscope. The fluorescence intensity was set as 1 after A23187 treatment. Values are mean ± SEM. *, $p < 0.01$ ($n = 15$). NT = no treatment; A23 = A23187.

inhibitor; Figure 3A), suggesting Src-dependent eNOS regulation upstream of Cav-1 S-nitrosylation.

Caveolin-1, the primary structural protein of caveolae, forms large homo- and heterooligomeric complexes that promote the self-assembly of caveolae (Sargiacomo *et al.*, 1995; Scherer *et al.*, 1997). Cav-1 oligomers are temperature-sensitive high-molecular-weight complexes that can be reduced to monomers (22 kDa) by exposing lysates to higher temperatures (see Western blot, Supplemental Figure 2). The ratio of Cav-1 monomers to oligomers after incubation at 60°C for 10 min was ~1:1, and thus we used this condition to assess changes in Cav-1 oligomer stability in situ.

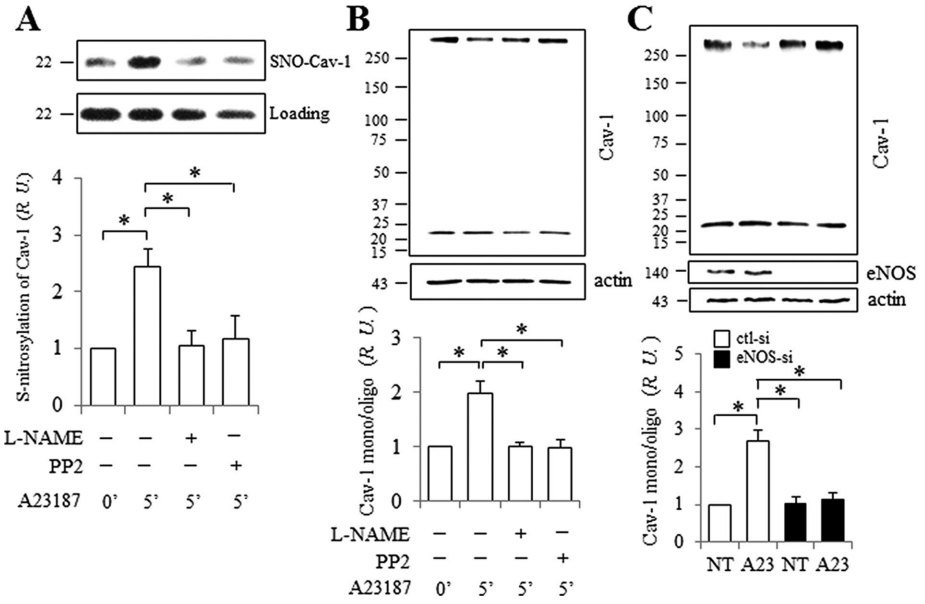

FIGURE 3: NO/Src dependent S-nitrosylation and monomerization of Cav-1. After pretreatment with 1 mM L-NAME or 15 μM PP2 for 30 min, HUVECs were stimulated for 5 min with 5 μM A23187 at 37°C. Cells were collected and Cav-1 S-nitrosylation (A) and oligomerization (B) were assessed as described in *Materials and Methods*. (A) Cav-1 S-nitrolysation in HUVEC induced by A23187 was blocked by pretreatment with L-NAME and PP2. Western blots probed with anti-Cav-1 after (top panel) and before (bottom panel, loading control) Biotin Switch assay. The ratio of nitrosated to total Cav-1 protein at time 0 was set as 1. Values are mean ± SEM. ∗, $p < 0.05$ ($n = 5$). (B) Inhibition of Cav-1 by L-NAME and PP2 in HUVECs stimulated with A23187. Western blots were probed with anti-Cav-1 (top panel) and anti-actin (bottom panel). Normalized ratios are shown in the bottom panel, and the ratio of monomers and oligomers of Cav-1 at time 0 was set as 1. Values are mean ± SEM. ∗, $p < 0.05$ ($n = 7$). (C) Monomerization of Cav-1 in HUVEC stimulated with A23187 was reduced when eNOS was depleted using 50 nM eNOS siRNA. The blots were probed for Cav-1 (top panel) and reprobed for eNOS and actin. The ratio of Cav-1 monomers and oligomers at time 0 (NT) in cells exposed to control siRNA was set as 1. Values are mean ± SEM. ∗, $p < 0.01$ ($n = 5$).

Phosphorylation of eNOS, Src, and Cav-1 can be induced by A23187, and Cav-1 phosphorylation is significantly reduced by pretreatment with L-NAME or PP2, indicating that Cav-1 Y14 phosphorylation increases following eNOS and Src activation (Chen *et al.*, 2012). Here, we assessed changes in the Cav-1 oligomer/monomer ratio under these same conditions. The monomer/oligomer ratio significantly increased (~2-fold) after treatment with A23187, and this was completely abolished by pretreatment of cells with either L-NAME or PP2 (Figure 3B). Neither L-NAME nor PP2 alone had an effect on Cav-1 oligomerization in serum-deprived cells (Supplemental Figure 3), indicating that the effect was stimulation-dependent. Furthermore, Cav-1 monomerization induced by A23187 was blocked by eNOS siRNA (Figure 3C). When these findings are taken together, Cav-1 S-nitrosylation is associated with the destabilization of Cav-1 oligomers in HUVEC via eNOS/NO/Src-dependent signaling.

eNOS-dependence of endothelial cell albumin and insulin uptake

We next investigated the effect of NO on albumin and insulin endocytosis in HUVEC (Figure 4). Following treatment with Cav-1, eNOS, or control siRNA, HUVEC were incubated with Alexa 488-BSA (bovine serum albumin) or -insulin for 30 min at 37°C and then washed extensively. Internalized fluorescent BSA or insulin appeared as puncta in cells exposed to control siRNA (Figure 4, A and B), whereas uptake (puncta) was reduced by 72% for BSA and 74% for insulin in cells transfected with Cav-1 siRNA, as expected. Interestingly, eNOS knockdown had a similar effect and reduced BSA uptake by 79% and insulin uptake by 68% (Figure 4, A–D), indicating that eNOS plays a significant role in caveola-mediated uptake in ECs. Infection of ECs with Adv-Cav-1-GFP after knockdown with Cav-1 siRNA rescued not only the expression of Cav-1, but also the expression of eNOS (Figure 4E) and the uptake of BSA and insulin (Figure 4, A and B) to levels similar to that observed in control siRNA-treated cells (Figure 4, A–D).

Signaling pathways associated with eNOS activation were next assessed in ECs treated with control versus eNOS-specific siRNA (Supplemental Figure 4A). ECs were incubated with 30 mg/ml BSA for times indicated, with and without knockdown of eNOS by siRNA (Supplemental Figure 4A). Phosphorylation of eNOS (Ser1177) was elevated significantly upon BSA stimulation (30 mg/ml) and was maximal at 30 min in control siRNA-treated cells. Interestingly, the increase in phosphorylation of both AKT (Ser473) and ERK (T202/Y204) induced by BSA were also significantly reduced when eNOS was depleted. Similarly, phosphorylation of AKT, ERK, and Cav-1 (pSer473-AKT, pT202Y204-ERK, and pY14-Cav-1) in ECs treated with 50 nM insulin was reduced in eNOS-depleted ECs (Supplemental Figure 4B). It is of note that Cav-1 expression level was not affected by eNOS knockdown (Figure 4E). Taken together, these experiments suggest that eNOS regulates Cav-1-dependent uptake of both albumin and insulin, as well as insulin-stimulated downstream AKT and ERK signaling, shown previously to play a role in NO production associated with caveola-mediated endocytosis of albumin (Maniatis *et al.*, 2006).

Semiquantitative Western blot analysis of eNOS and Cav-1 expression in endothelial cells

To better understand the stoichiometry of Cav-1-dependent regulation of eNOS expression and activity, and vice versa, the relative expression of both in ECs was determined using Cav-1-YFP, eNOS-YFP, eNOS, and Cav-1 overexpressed in HEK cells as "internal" standards (Figure 5). Cell lysates from HUVEC, WT-HEK cells, and HEK cells transfected with Cav-1-YFP, eNOS-YFP, Cav-1, and eNOS cDNA were assessed by Western blotting. The blot was first probed with anti-GFP antibody to quantify YFP-tagged proteins (Figure 5A); eNOS-YFP and Cav-1-YFP showed similar levels of expression. The same blot was then stripped and reprobed for Cav-1 (Figure 5B). Surprisingly, Cav-1 expression in HUVEC was much higher (~2.5-fold) than in the HEK/Cav-1-YFP expression model, demonstrating that Cav-1 expression is indeed abundant in ECs. The blot was then reprobed with anti-eNOS antibody (Figure 5C), and expressed eNOS levels in the HEK/eNOS-YFP and HEK/eNOS cell lines were similar. However, this level was much higher than that of the eNOS observed in HUVEC, which was barely visible (Figure 5C). To further assess the eNOS expression level, HEK/eNOS cell lysates were serially diluted to create a standard curve in the Western blots,

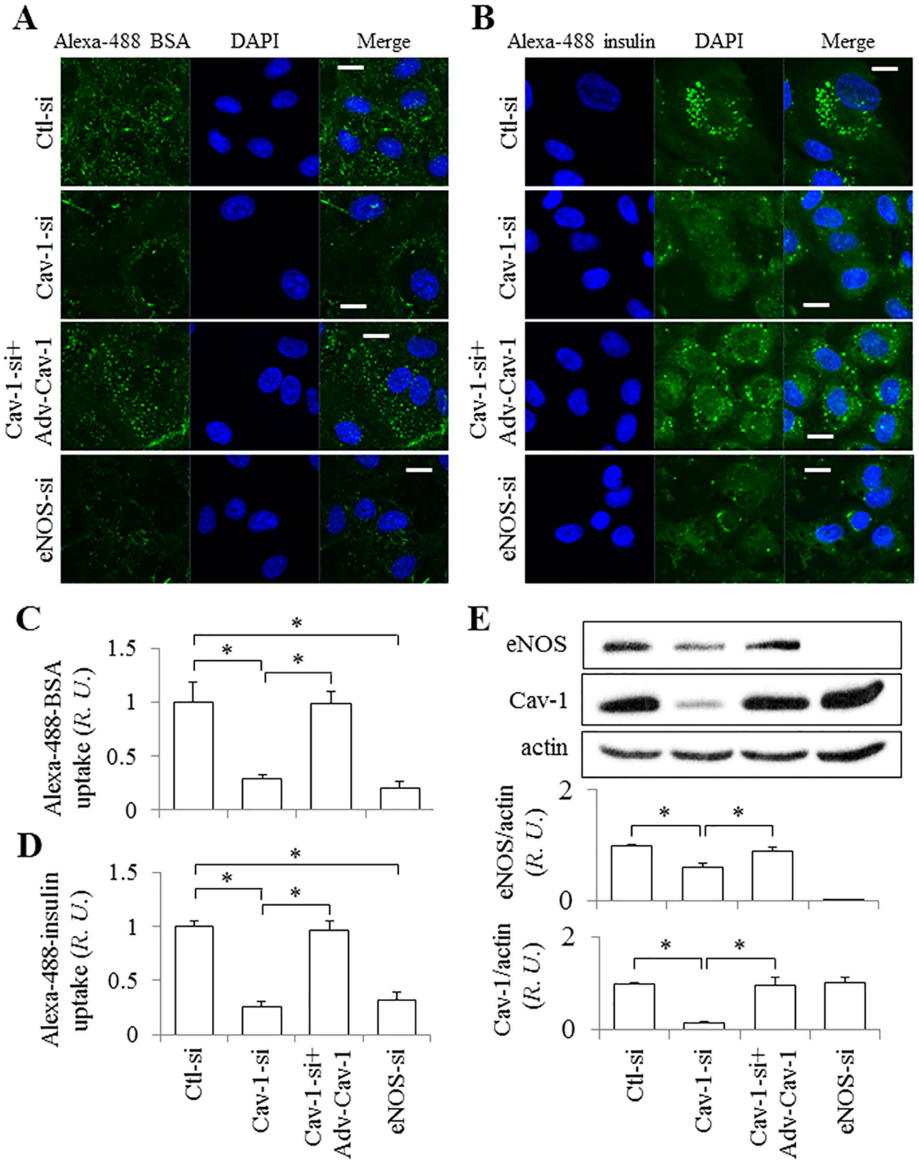

FIGURE 4: Effect of eNOS on albumin and insulin uptake. HUVECs on glass coverslips were treated with control siRNA or Cav-1 siRNA (100 nM) with and without rescue by Adv-Cav-1 transfection, or with eNOS siRNA (50 nM), and then exposed to Alexa 488–conjugated BSA (A) or insulin (B) for 30 min at 37°C, fixed, and prepared for confocal microscopy. Bar, 10 μm. (C, D) Normalized values of BSA and insulin uptake in HUVEC. The fluorescence intensity of internalized BSA in cells exposed to control siRNA was set as 1. Values are mean ± SEM. *, $p < 0.05$ vs. control siRNA ($n = 10$ from at least three independent experiments). (E) Western blot shows expression level of eNOS and Cav-1 in HUVECs treated with control siRNA, Cav-1 siRNA with and without rescue by Adv-Cav-1 transfection, or eNOS siRNA. Normalized values are shown in the bottom panel. The ratio of eNOS or Cav-1 to actin in cells exposed to control siRNA was set as 1. Values are mean ± SEM. *, $p < 0.05$ ($n = 4$).

which was used to assess eNOS expression in HUVECs (see Supplemental Figure 5, A and B, for further details). Final analysis showed that there was 80-fold more eNOS in HEK/eNOS cells than in HUVECs (Supplemental Figure 5C). Finally, the blot was reprobed for actin (Figure 5D) to normalize each protein band, and eNOS expressed in HUVEC was set as 1 (Figure 5E). Monomeric Cav-1 expression in HUVEC and HEK/Cav-1-YFP cells was 200-fold and 95-fold greater than that of eNOS in HUVEC, respectively; monomeric eNOS in HEK/eNOS-YFP and HEK/eNOS cells was 79- and 80-fold greater than that in HUVEC, respectively (Figure 5E). Thus, the semiquantitative ratio of Cav-1 to eNOS expression in HUVEC was ~200:1, which suggests that in ECs, Cav-1 is 200-fold more abundant than eNOS, which is even more than is achieved by overexpression of Cav-1-YFP in HEK/eNOS cells. The localization of Cav-1 and eNOS in transfected HEK cells is shown by confocal imaging in Figure 5F.

siRNA depletion of Cav-1 reduces eNOS expression level but increases its activity

Because Cav-1 is highly expressed in ECs relative to eNOS, and eNOS is known to reside in part at the plasma membrane (PM) on or near caveolae (Liu *et al.*, 1996; Maniatis *et al.*, 2006), we hypothesized that in addition to regulating the activity of eNOS in ECs, Cav-1 may regulate its expression as well.

Following the delivery of increasing amounts of Cav-1 siRNA for 72 h, Cav-1 protein level was dose-dependently reduced (Figure 6, A and B). Interestingly, eNOS expression also decreased by ~70% following treatment with 120 nM Cav-1 siRNA, whereas VE-cadherin, β-catenin, and Src protein levels were not different. These results are supported by immunostaining and confocal imaging (Figure 6C), which showed reduction in eNOS staining upon Cav-1 depletion. A similar reduction in eNOS was obtained when other Cav-1 siRNAs were tested (Supplemental Figure 6), indicating that the eNOS expression level is regulated by Cav-1 per se, rather than nonspecifically down-regulated by Cav-1 siRNA. eNOS knockdown, however, did not alter Cav-1 expression, as observed by confocal microscopy and Western blotting (Figures 6C and 4E).

eNOS activity was also assessed in Cav-1-depleted ECs (Figure 7). After treatment with 100 nM Cav-1 siRNA for 72 h, ECs were stimulated with 5 μM A23187, cell lysates were collected, and Western blotting was performed (Figure 7A). Both Cav-1 and eNOS expression levels declined (Figure 7B); however, the ratio of p-eNOS to total (t) eNOS in Cav-1 siRNA–treated ECs was significantly increased compared with that in control siRNA–treated ECs, even at time 0 (Figure 7C). Thus, Cav-1 inhibits eNOS basally. However, Cav-1-dependent inhibition of eNOS phosphorylation 3 min after A23187 treatment was eightfold that at time 0 (gray bars in the inset of Figure 7C). To further characterize this observation, cell supernatants following A23187 treatment were collected for nitrate (NO_2^-) measurement, and eNOS activity was calculated per minute relative to total eNOS expression. As expected, NO_2^- production was greater per molecule of eNOS in ECs after Cav-1 depletion (Figure 7D). Cav-1 inhibition of eNOS activity was maximal 1 min after A23187 stimulation (inset of Figure 7D). When these findings are taken together, due to its location on caveolae, eNOS expression level and activity are tightly regulated by Cav-1.

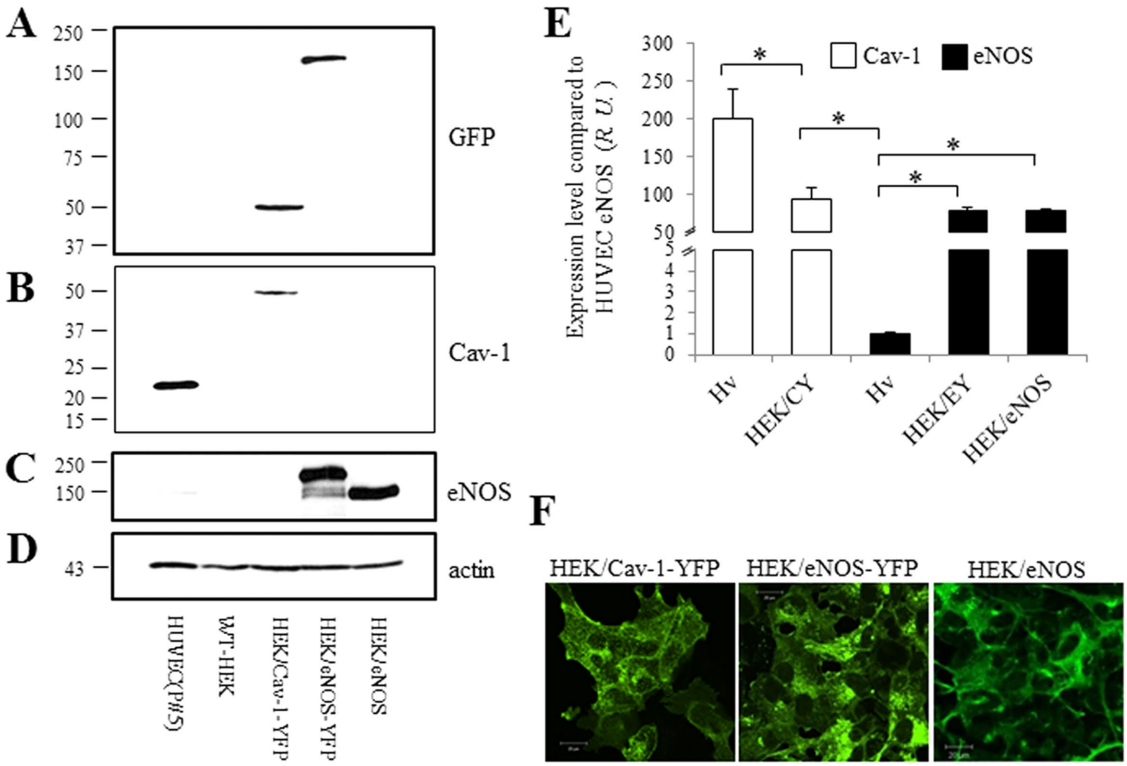

FIGURE 5: Comparison of Cav-1 and eNOS expression in HUVECs. Equal amounts of total lysate from HUVECs (fifth passage), WT-HEK cells, and HEK cells transfected with Cav-1-YFP, eNOS-YFP, and eNOS cDNAs were prepared for Western blot. The blot was first probed with anti-GFP antibody (A) and then the same blot was stripped and reprobed for Cav-1 (B), eNOS (C), and finally actin (D). (E) Band intensities were normalized to eNOS in HUVEC. The ratio of eNOS/actin was set as 1. Values are mean ± SEM. *, $p < 0.05$ ($n = 4$). (F) Representative confocal images of Cav-1-YFP, eNOS-YFP, and eNOS cDNAs transfected in HEK cells from at least three independent experiments. Scale bar, 20 μm.

Effect of Cav-1 on eNOS expression and activity in HEK/eNOS cells

To further assess the role of Cav-1 in the regulation of eNOS, HEK cells stably expressing eNOS were transfected with different amounts of Cav-1-GFP cDNA, since HEK cells express very little native Cav-1 protein. As the amount of transfected Cav-1-GFP increased (Figure 8, A and B), the eNOS expression level initially increased (with 0.2 μg Cav-1-GFP cDNA) and peaked at approximately twofold (with addition of 0.6 μg Cav-1-GFP cDNA). However, overexpression of Cav-1-GFP (up to 8.0 μg) reduced eNOS expression (Figure 8C). Previous reports suggest that GFP-conjugates of proteins, including caveolin-1, may impact oligomerization and expression (Hayer *et al.*, 2010; Han *et al.*, 2015). To test whether the GFP tag associated with Cav-1 played a role in modulating eNOS expression, Myc-tagged Cav-1 was transfected into HEK/eNOS cells instead of Cav-1-GFP cDNA. As observed in Supplemental Figure 7, Myc-Cav-1 had the same effect on eNOS expression as GFP-tagged Cav-1. In parallel with its expression level, eNOS activity displayed a similar biphasic pattern, first increasing at lower doses of transfected Cav-1 cDNA (maximum at 0.6 μg) and then decreasing with higher doses of transfected Cav-1 cDNA (8.0 μg; Figure 8D). These data suggest that lower levels of Cav-1 stabilize eNOS expression, whereas higher levels inhibit eNOS expression and activity.

DISCUSSION

In this study, we demonstrate that vascular endothelial cell eNOS and Cav-1 expression are significantly reduced in subjects with T2DM. Using in vitro cell culture models, we assessed the molecular determinants of reciprocal Cav-1 and eNOS regulatory mechanisms. The Cav-1 expression level in ECs, determined semiquantitatively by Western blotting, was shown to be 200-fold greater than that of eNOS. Depletion of Cav-1 using siRNA reduced the expression of eNOS protein, which is known to localize to the plasma membrane (PM) via acylation (Liu *et al.*, 1996; Michel and Michel, 1997; Prabhakar *et al.*, 2000) and on caveolae via direct interaction with Cav-1 (Bernatchez *et al.*, 2005; Maniatis *et al.*, 2006), indicating that Cav-1 helps to stabilize eNOS expression. In cells with reduced Cav-1 expression, eNOS activity per molecule increased, suggesting that Cav-1 also plays a critical role as a basal inhibitor of eNOS activity, as reported previously (Bernatchez *et al.*, 2005; Chen *et al.*, 2012). Overexpression of eNOS in HEK cells (which normally do not express eNOS), and then transfection with increasing amounts of Cav-1 cDNA showed that eNOS, through an NO-mediated Src signaling pathway, plays a critical role in promoting Cav-1 functions such as caveola-mediated endocytosis of albumin and insulin. This effect of eNOS may be direct, due to S-nitrosylation of Cav-1 Cys156 (Bakhshi *et al.*, 2013), or via NO-mediated Src activation and subsequent phosphorylation and destabilization of Cav-1 oligomers (Chen *et al.*, 2012; Zimnicka *et al.*, 2016). Disruption of this tightly coupled reciprocal regulatory mechanism via depletion of Cav-1 and/or eNOS may to be linked to vascular complications of disease, such as diabetic vascular dysfunction (Moroi *et al.*, 1998; Cohen *et al.*, 2003; Murata *et al.*, 2007; Mahmoud et al., 2016) and insulin resistance (Wang *et al.*, 2015), pulmonary hypertension (Bakhshi *et al.*, 2013), nitrate tolerance (Mao *et al.*, 2014), and inflammation-induced pulmonary vascular remodeling (Oliveira *et al.*, 2017).

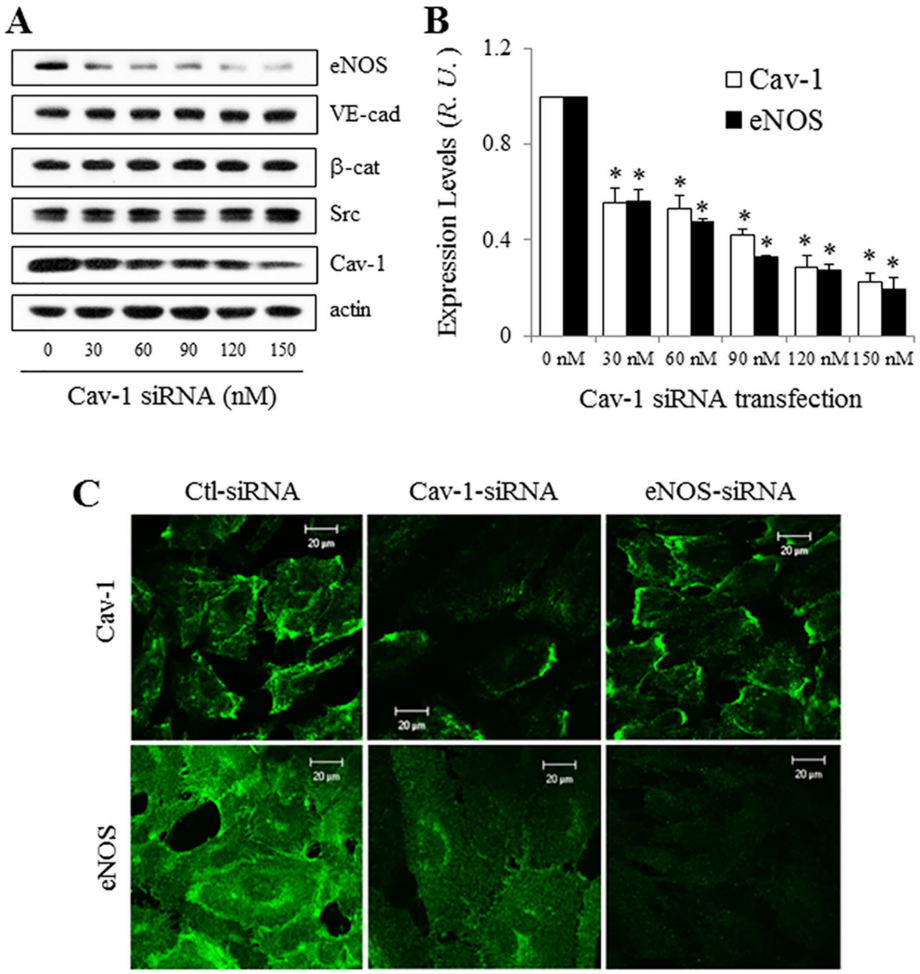

FIGURE 6: eNOS expression decreased in HUVECs treated with Cav-1 siRNA. (A) HUVECs were treated with 0–150 nM Cav-1 siRNA for 72 h and collected for determination of eNOS, VE-cadherin, β-catenin, Src, Cav-1, and actin expression by Western blot. (B) Reduced eNOS expression level in HUVECs following Cav-1 knockdown. Band intensities in A were normalized, and the ratio between Cav-1 and actin after treatment with 0 nM siRNA was set as 1. Values are mean ± SEM. ∗, $p < 0.05$ vs. 0 nM siRNA ($n = 4$). (C) Confocal images (at least three independent experiments) of Cav-1 (top panel) and eNOS (bottom panel) in HUVEC treated with siRNA of control, Cav-1, or eNOS. Scale bar, 20 μm.

eNOS is reportedly regulated by various proteins in different subcellular locations; for example, Ca^{2+}/calmodulin-mediated activation of eNOS is mainly effective at the PM, whereas AKT-driven activation of eNOS is most pronounced in the Golgi (Fulton *et al.*, 2004; Zhang *et al.*, 2006). We show here that eNOS translocates to the EC plasma membrane, where it colocalizes with the adherens junction protein β-catenin upon stimulation with the Ca^{2+} ionophore A23187. Consistent with the above findings, phosphorylated eNOS (pSer1177), a positive regulator of eNOS activity (Fulton *et al.*, 1999; Scotland *et al.*, 2002), also colocalizes with β-catenin, indicating that activated eNOS localizes to cell–cell junctions, where it may affect junctional integrity and endothelial barrier function (Govers *et al.*, 2002). Because NO is an extremely reactive signaling molecule, production needs to be tightly regulated (Dröge, 2002; Oritz and Garvin, 2003; Bonini *et al.*, 2014). Our experiments show that eNOS translocation to the PM and colocalization with Cav-1 following its activation likely play an important role in eNOS inactivation, confirming previous observations (Ju *et al.*, 1997; Michel *et al.*, 1997; Chen *et al.*, 2012; Trane *et al.*, 2014).

Previously, we showed by both co-immunoprecipitation and Förster resonance energy transfer (FRET) that pSer1177 eNOS preferentially interacts with Cav-1 phosphorylated on Tyr14 (Chen *et al.*, 2012). Thus, following eNOS activation, NO-mediated activation of Src kinase and subsequent phosphorylation of Cav-1 Tyr14 promote the rapid inactivation of eNOS at the PM by direct binding to the exposed caveolin scaffolding domain (CSD). eNOS-depletion in ECs further supports the hypothesis that eNOS-derived NO promotes a conformational change in Cav-1 that serves as a negative-feedback regulatory mechanism to maintain vascular homeostasis.

Cav-1, a membrane-inserted hairpin protein of 22 kDa molecular weight, forms homooligomers via interaction of N-terminal residues 61–101 and C-terminal Cys156 (Song *et al.*, 1997; Bakhshi *et al.*, 2013). We observed that oligomerization of Cav-1 can be disrupted in a temperature-dependent manner (Supplemental Figure 1), enabling the ratio of Cav-1 monomers/oligomers to be used as an index of posttranslational modification. NO produced by eNOS can react with thiol groups on nearby proteins (S-nitrosylation) and thereby modulate a variety of cellular processes such as protein trafficking, redox state, endothelial permeability, and cell cycle (Iwakiri, 2011; Durán *et al.*, 2013). In HUVEC, A23187-induced Cav-1 Cys156 S-nitrosylation, Cav-1 Tyr14 phosphorylation, and destabilization of Cav-1 oligomers could be blocked by either eNOS or Src inhibition. Similar results were reported in human lung microvascular endothelial cells treated with TNF-α (Bakhshi *et al.*, 2013) and albumin (Zimnicka *et al.*, 2016).

Cav-1 Cys156 S-nitrosylation and Tyr14 phosphorylation destabilize Cav-1 oligomers (Bakhshi *et al.*, 2013; Zimnicka *et al.*, 2016); however, the impact of these modifications on the conformation of oligomers and monomers is not yet clear. Computer modeling of the Cav-1 structure predicted that when Cav-1 Tyr14 is phosphorylated, there will be movement of the N-terminal region that may reorient the nearby Cav-1 scaffolding domain (SCD) to create an interface that favors interaction with other proteins containing the Cav-1-binding motif (ΦXXXXΦXXΦ; Couet *et al.*, 1997). In support of this modeling conclusion, we showed that phosphorylated Cav-1 Tyr14 exhibits greater binding to eNOS (Chen *et al.*, 2012). Potentially, charged Glu10, Glu20, and Arg19 residues near pTyr14-Cav-1 may repel other molecules of pY14-Cav-1, resulting in a decrease in the oligomerization domain (aa 61–101)– and scaffold domain (aa 82–101)–dependent binding of Cav-1 to itself (Song *et al.*, 1997; Zimnicka *et al.*, 2016).

Recently, we observed in HEK293 cells cotransfected with wild-type, Y14D, or Y14F Cav1-CFP and Cav1-YFP constructs that FRET efficiency was greater with Y14F pairs than with Y14D pairs, indicating that pY14-Cav1 regulates the spatial organization of Cav1 molecules within the oligomer (Zimnicka *et al.*, 2016). In addition,

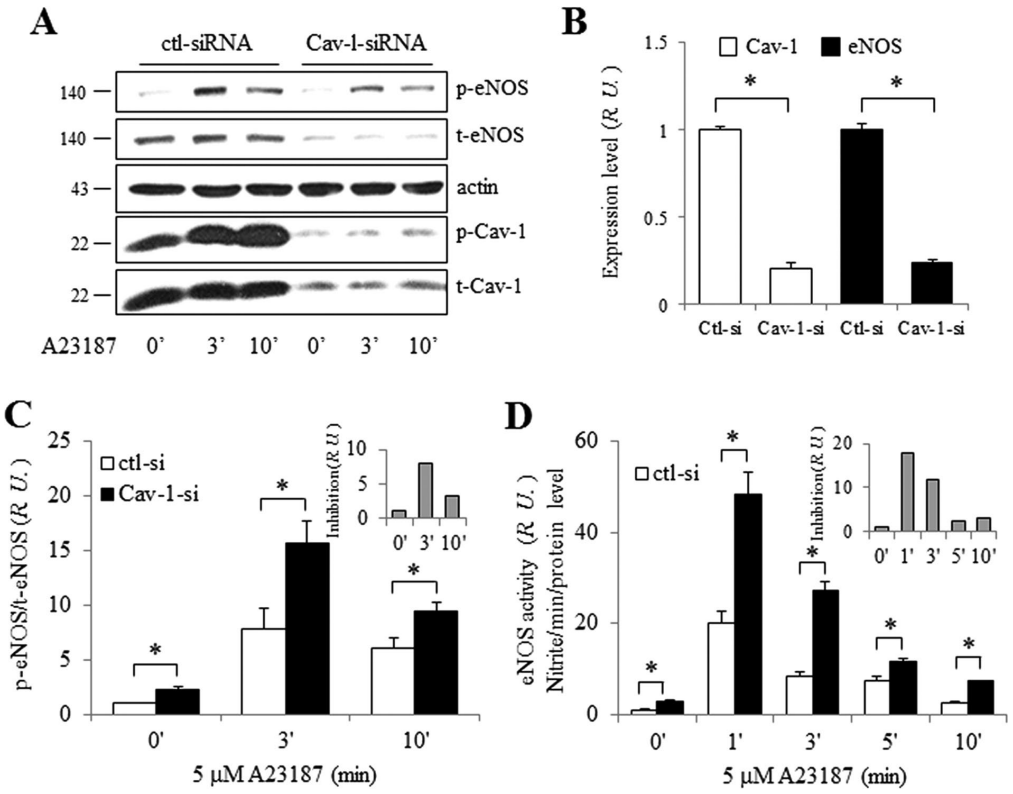

FIGURE 7: eNOS expression and activity after Cav-1 knockdown in HUVECs. (A) A23187 induced p-eNOS Ser1177 and p-Cav-1 Tyr14 in HUVECs transfected with Cav-1 siRNA (100 nM). (B) Normalized expression levels of total Cav-1 and eNOS. Values are mean ± SEM. *, $p < 0.001$ ($n = 6$). (C) Normalized eNOS phosphorylation from panel A. Ratio of p-eNOS/t-eNOS at 0 min was set as 1. Cav-1 inhibition of p-eNOS induced by A23187 is shown in the inset (gray bars). Values are mean ± SEM. *, $p < 0.05$ ($n \geq 6$). (D) NO release from HUVECs transfected with Cav-1 siRNA. eNOS activity (nitrite accumulation per min normalized to eNOS expression level at time 0 in control siRNA-treated cells) was set as 1. Cav-1 inhibition of eNOS induced by A23187 is shown in the inset (gray bars). Values are mean ± SEM. *, $p < 0.05$ ($n = 6$).

albumin-induced Src activation or direct activation of Src using a rapamycin-inducible Src construct (RapR-Src) led to an increase in monomeric Cav1 in Western blots, as well as a simultaneous increase in vesicle number and a decrease in FRET intensity. These data indicate that phosphorylation of Cav-1 leads to separation or "spreading" of neighboring negatively charged N-terminal phosphor–tyrosine residues (Zimnicka *et al.*, 2016). Furthermore, sustained phosphorylation of the N-terminus may facilitate Cav-1 ubiquitination of Lys86 in the scaffolding domain, resulting in Cav-1 degradation via the proteasome (Bakhshi *et al.*, 2013; Mao *et al.*, 2014).

Cav-1-dependent endocytosis and transcytosis of plasma macromolecules such as insulin, oxidized low-density lipoprotein (oxLDL), and albumin by ECs has been extensively studied (Tiruppathi *et al.*, 1997; Minshall *et al.*, 2000; Shajahan *et al.*, 2004; Frank *et al.*, 2008; Wang *et al.*, 2011, 2015; Pavlides *et al.*, 2014; Zimnicka *et al.*, 2016). Also, while mice that lack Cav-1 are protected from atherosclerosis (Fernández-Hernando *et al.*, 2009), they are prone to develop type 2 diabetes (Wang *et al.*, 2011), neuropathology associated with aging (Head *et al.*, 2010), and capillary rupture in severe hypertension (Maniatis *et al.*, 2008; Cheng *et al.*, 2015). Consistent with previous studies (Sverdlov *et al.*, 2009; Pavlides *et al.*, 2014; Wang *et al.*, 2015), we showed that knockdown of Cav-1 in ECs significantly reduced albumin and insulin uptake. Interestingly, we also showed that depletion of eNOS significantly reduced uptake of albumin and insulin, as well as the phosphorylation AKT Ser473 and ERK T202/Y204, supporting the concept that caveolae-mediated endocytosis in ECs is mediated in part by an eNOS/PI3K/AKT/ERK signaling pathway (Schubert *et al.*, 2001; Maniatis *et al.*, 2006; Wang *et al.*, 2011).

The ratio of Cav-1 to eNOS protein expression in HUVECs determined by semiquantitative Western blotting was 200:1, suggesting that Cav-1 overexpression relative to eNOS may have important implications. eNOS is found associated with the PM through acylation (Liu *et al.*, 1996; Michel and Michel, 1997; Prabhakar *et al.*, 2000) and is enriched on caveolae (Maniatis *et al.*, 2006). As shown here, when Cav-1 is depleted in ECs, eNOS localization in the membrane is disrupted and its expression is also reduced. The opposite, however, was not true; eNOS depletion had no effect on Cav-1 expression. Surprisingly, although the eNOS level was reduced following Cav-1 knockdown, its phosphorylation and activity per molecule were increased, indicating that Cav-1 also plays a key role in the basal inhibition of eNOS activity. *Cav-1*$^{-/-}$ mice exhibit pulmonary and cardiac hypertrophy (Drab *et al.*, 2001; Razani *et al.*, 2001; Zhao *et al.*, 2002; Maniatis *et al.*, 2008), and eNOS-overexpressing transgenic (eNOS-Tg) mice are hypertensive. These data support the notion that excessive endothelium-derived NO or NO_x production when the Cav-1/eNOS ratio is low may impair cardiovascular homeostasis (Mao *et al.*, 2014; Godo *et al.*, 2016; Oliveira *et al.*, 2017). Thus, an important function of Cav-1 is to maintain normal vessel function through its ability to modulate NO production under normal physiological conditions (Jia and Sowers, 2015). When Cav-1 protein expression is reduced, eNOS becomes hyperphosphorylated and hyperactivated, leading to vascular dysfunction, as

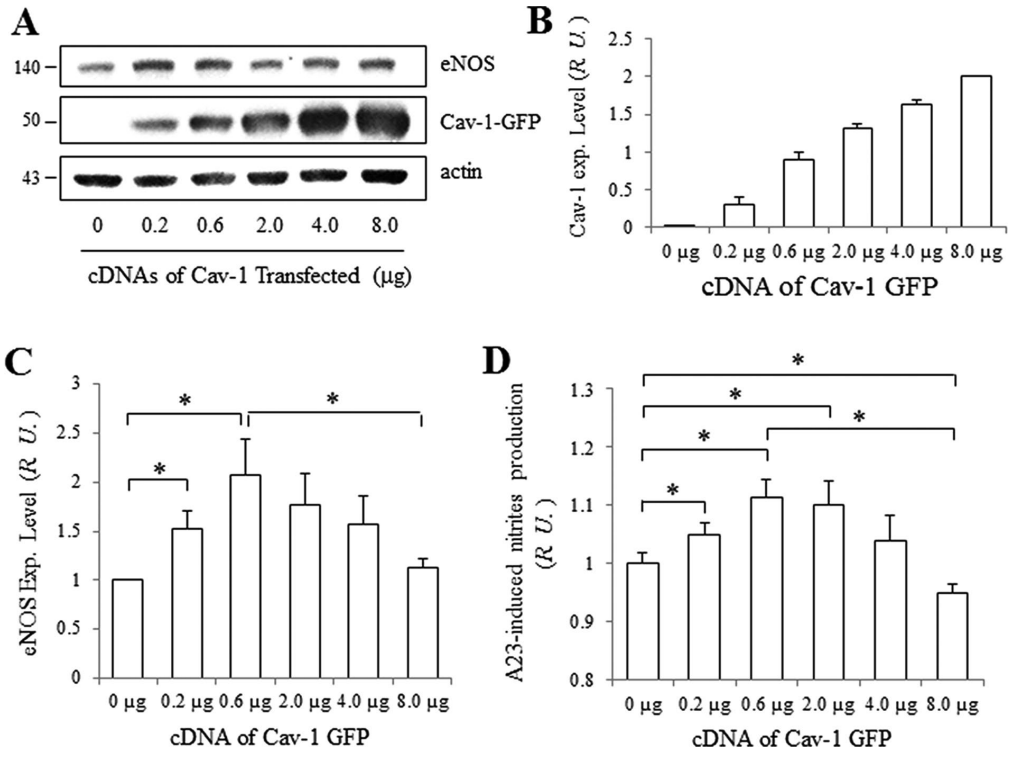

FIGURE 8: eNOS expression and activity is regulated by Cav-1 in HEK/eNOS cells. (A) Expression level of eNOS in HEK/eNOS cells following transfection with Cav-1-GFP cDNA. A total of 8 μg of cDNA (balanced with control plasmids) were transfected into HEK/eNOS cells. After 48 h, the cells were collected and blotted for eNOS, Cav-1, and actin. (B) Normalized expression level of Cav-1-YFP and (C) eNOS. Values are mean ± SEM. *, $p < 0.05$ ($n = 5$). (D) NO release from HEK/eNOS cells after transfection with different doses of Cav-1-GFP cDNA. After treatment of HEK/eNOS cells with 5 μM A23187 for 45 min at 37°C, the supernatants were analyzed for total nitrite level. Total nitrite normalized to eNOS level in cells transfected with 0 μg Cav-1-GFP was set as 1. Values are mean ± SEM. *, $p < 0.05$ ($n = 3$).

observed in ECs in donor lungs from patients with idiopathic pulmonary arterial hypertension (Bakhshi *et al.*, 2013), T2DM (Mahmoud *et al.*, 2016), and ARDS (Oliveira *et al.*, 2017).

In conclusion, we have elucidated a heretofore unappreciated reciprocal regulatory relationship between eNOS and Cav-1 in ECs. On one hand, Cav-1 inhibits eNOS activity through direct binding (which was known), but we also demonstrated that Cav-1 regulates eNOS expression level, implicating Cav-1 expression as an important determinant of endothelial vasodilatory and homeostatic functions (Frank *et al.*, 2003; Sowa, 2012). On the other hand, eNOS-derived NO-production and activation of Src kinase induce pY14-Cav-1–dependent endocytosis of albumin and insulin (Maniatis *et al.*, 2006; Pavlides *et al.*, 2014; Wang *et al.*, 2015), while sustained NO production and persistent Cav-1 S-nitrosylation lead to Cav-1 ubiquitination and degradation (Hayer *et al.*, 2010; Bakhshi *et al.*, 2013). The molecular and structural determinants that dictate how Cav-1 and eNOS regulate one another's function in ECs, how vascular dysfunction due to their depletion contributes to cardiovascular disease (Li *et al.*, 2006; Pavlides *et al.*, 2014), and finally how to reverse the process to restore vascular homeostasis await further interrogation and translation.

MATERIALS AND METHODS

Human subjects

A cross-sectional cohort of human subjects was employed to validate a mechanistic phenotype of vascular disease. Two groups of participants were recruited, a T2DM group ($n = 8$; age = 58 ± 4 yr; BMI = 34.1 ± 2.1 kg/m^2) and a LHC group ($n = 10$; age = 27 ± 1 yr; BMI = 22.3 ± 1.1 kg/m^2). The LHC group was selected to represent a state of optimal health to which the diseased T2DM group could be compared. Full experimental procedures from larger study cohorts have been presented previously (Williamson *et al.*, 2015; Mahmoud *et al.*, 2016; Mey *et al.*, 2018). Briefly, participants were recruited from the Chicago, IL, metropolitan area, and all subjects were screened via health history, medical exam, resting EKG, and fasting blood chemistry in the Clinical Research Centers of the University of Illinois at Chicago. Glucose tolerance was characterized by a 75 g oral glucose tolerance test (OGTT) following a standard fasting period for all subjects. Individuals were excluded if they used nicotine, had undergone greater than 2 kg weight change in the past 6 mo, or had evidence of hematological, renal, hepatic, or overt CVD. LHCs were excluded if results of OGTT indicated impaired fasting glucose or impaired glucose tolerance. T2DM subjects self-reported diabetes duration of 4 ± 1 yr. On a separate visit and following a 12-h fast, skeletal muscle biopsies of the vastus lateralis were obtained under local anesthetic (lidocaine HCl 1%) using a 5-mm Bergstrom cannula with suction. Muscle tissue was blotted, trimmed of adipose and connective tissue if necessary, and immediately (less than 90 s from extraction) flash frozen in liquid nitrogen and subsequently stored at –80°C for future processing and analysis. All studies were approved by the Institutional Review Boards of the University of Illinois at Chicago and performed in accordance with the Declaration of Helsinki. Written informed consent was obtained from all research participants during the initial screening visit.

Cell culture and transfection

HUVECs and growth medium (EGM-2 plus Bullet kit) were from Lonza. HEK293 cells were from the American Type Culture Collection (ATCC). DMEM (for HEK293 cells) was from Invitrogen. Fetal bovine serum (FBS) was from Serum Source International. Geneticin was purchased from Invitrogen.

HUVECs were cultured in EGM-2 (Lonza) supplemented with 10% (vol/vol) FBS, split 1:4 upon reaching confluence, and used at passage 5. For immunofluorescence microscopy, cells were grown on gelatin-coated glass coverslips. HEK293 cells were cultured in DMEM supplemented with 10% FBS and 1% penicillin/streptomycin. cDNAs of Cav-1 or eNOS constructs as described previously (Chen *et al.*, 2012) were transfected in HEK293 cells with Lipofectamine 2000 according to the manufacturer's instructions. Stable cell lines were obtained by single-cell sorting onto a 96-well plate. Cells with fluorescent tags were verified by fluorescence microscopy and immunoblot analysis.

Reagents

PP2 (4-amino-5-(4-chlorophenyl)-7-(*t*-butyl) pyrazolo [3, 4-*d*] pyrimidine), the calcium ionophore A23187, and N^G-nitro-L-arginine methyl ester (L-NAME) were from Sigma. n-Octyl-β-D-glucopyranoside (ODG) was from RPI Corp. An S-nitrosylated protein detection kit was from Cayman Chemical. siRNAs for eNOS and transfection reagent DharmaFect 1 were from Dharmacon. Control siRNA and two Cav-1 siRNAs were purchased from Santa Cruz Biotechnologies. The sequence of the first (#1) Cav-1 siRNA was sense• 5-AACCAGAAGGGACACACAG-3′ and antisense 5′-CUGUGUGUCCCUUCUG-GUU-3′, and the second (#2) was a pool of three different siRNA duplexes (A: sense: 5′-GUUCCAAGUUGCUAAUACAtt-3′, antisense: 5′-UGUAUUAGCAACUUGGAACtt3′; B: sense: 5′-CUUCUCAUGAUCCAACUAAtt-3′, antisense: 5′-UUAGUUGGAUCAUGAGA-AGtt-3′; C: sense: 5′-CAUGUCUGUUCUACAUAGAtt-3′, antisense: 5′-UCUAUGUAGAACAGACAUGtt-3′). Adenovirus (Ad) Cav-1-GFP and control Ad-GFP were kindly provided by Hemal Patel, University of California, San Diego. Dynabeads M-280 streptavidin, 4′,6-diamidino-2-phenylindole (DAPI), Lipofectamine 2000, mammalian expression vectors pcDNA3 and pcDNA6, Alexa 488–conjugated bovine serum albumin (BSA), and all fluorescently labeled secondary antibodies were purchased from Invitrogen. Alexa fluor 488 labeled insulin was from NANOCS. Vectors for YFP were obtained from Clonetech. Mouse anti-eNOS, rabbit anti-caveolin-1, mouse anti-pY14-Cav-1, rabbit and mouse immunoglobulin G, and mouse anti-actin were from BD Biosciences. Rabbit anti-phospho-eNOS (pSer1177), rabbit anti-phospho-AKT (pSer473), rabbit anti-phospho-ERK, rabbit anti-AKT, rabbit anti-phospho-ERK (pT202/Y204), and rabbit anti-ERK antibodies were from Cell Signaling Technology. Rabbit anti-Myc antibody was from Abcam. Goat anti-β-catenin antibody is from MyBiosources. Nitrocellulose membrane was from Bio-Rad Laboratories. The SuperSignal West Femto Kit and Restore Western Stripping buffer were from Pierce.

Construction of Cav-1 and eNOS plasmids

Cav-1 and eNOS plasmid constructs with and without fluorescent tags were as described previously (Chen *et al.*, 2012; Zimnicka *et al.*, 2016). Human caveolin-1 WT cDNA in pcDNA 3.1 (Minshall *et al.*, 2000) was subcloned into pcDNA6 containing 6 Myc and histidine tags.

Immunohistochemistry and confocal microscope

Confluent monolayers of cells grown on coverslips were serum-starved, treated with reagents, and fixed for 20 min at room temperature with 4% paraformaldehyde in PBS containing 0.12 M sucrose as described previously (Chen *et al.*, 2006). Briefly, the fixed cells were blocked by incubation for 1 h with 5% normal goat serum in PBS containing 0.2% BSA and 0.1% Triton X-100 at room temperature, and then the cells were incubated at 4°C overnight with primary antibody. Next, the cells were incubated for 1 h at room temperature with secondary antibody (Alexa 568, Alex 488, or Alexa 647 conjugates) in PBS containing 2% normal goat or donkey serum, 1% BSA, and 0.1% Triton X-100. The cells were further stained with DAPI in PBS for 20 min at room temperature. Finally, the coverslips were mounted on glass slides. Fluorescent images were obtained using a Zeiss LSM 880 confocal microscope.

Biotin switch assay: S-nitrosylation of Cav-1

S-nitrosylation of Cav-1 was detected by the biotin switch method as described previously (Jaffrey and Snyder, 2001; Bakhshi *et al.*, 2013). Briefly, after serum starvation for 3–5 h, endothelial cells were treated with 5 µM A23187 (with or without 30 min pretreatment with 1 mM L-NAME or 15 µM PP2) for 5 min. The cells were then collected and cell lysates were immunoprecipitated with streptavidin-conjugated antibodies and pulled down with streptavidin beads. Biotinylated Cav-1 was resolved by SDS–PAGE. The same samples prior to immunoprecipitation were used as loading controls.

Western blotting and Cav-1 oligomerization

After treatment with different reagents, cells were lysed by sonication in 2% ODG in Tris buffer (pH 7.50, 50 mM Tris, 150 mM NaCl, 1 mM NaF, 1 mM EDTA, 1 mM Na_3VO_4, 44 µg/ml phenylmethylsulfonyl fluoride [PMSF], 1% protease inhibitor cocktail). The lysates were centrifuged for 20 min at 16,000 × *g* at 4°C. The supernatants were collected for Western blotting.

For Cav-1 oligomerization, confluent HUVECs were serum starved for 3–4 h and then treated for indicated times. Loading buffer and DTT were added to the same amount of sample and incubated for 10 min at 60°C. Finally, the samples were run on 8–12% gradient SDS–PAGE gels for Western blot analysis.

siRNA-mediated Cav-1 and eNOS Depletion

HUVECs were cultured to ~80% confluence and transfected with eNOS (50 nM), Cav-1 (100 nM), or scrambled siRNA (100 nM). After 24 h, cells were transferred to glass coverslips and cultured for another 2 d for confocal immunostaining slides, or to six-well plates for Western blotting experiments.

Ad-Cav-1 transfection in endothelial cells

Rescue of Cav-1 expression was tested, and the best time was shown to be 24 h after transfection with Ad-Cav-1 compared with control Ad-GFP (unpublished data) as described previously (Li *et al.*, 2003). Briefly, medium containing Ad-Cav-1 was added to ECs 48 h after transfection with siRNA, and the cells were cultured for another 24 h prior to experiments.

Fluorescently labeled albumin and insulin uptake in endothelial cells

For BSA and insulin uptake experiments, confluent HUVECs were grown on gelatin-coated glass coverslips as described previously (Sverdlov *et al.*, 2009; Wang *et al.*, 2011). Briefly, ECs were starved for 5 h in basal EBM2 and incubated with 10 µg/ml Alexa 488–conjugated BSA in basal media containing 0.1 mg/ml unlabeled BSA or 50 nM Alexa 488–labeled insulin for 30 min at 37°C. Cells were washed with acid wash buffer, pH 2.5, and then with Hank's balanced salt solution (HBSS) to remove surface-bound BSA or insulin, fixed with 4% paraformaldehyde, and stained with the

nuclear marker DAPI (1 μg/ml). For quantification of uptake in siRNA-transfected cells, at least 10 images of equal area were acquired, and each experiment was repeated three times. The uptake percentage was assessed from thresholded images using the ImageJ Particle Analysis module.

Phosphoryation of eNOS (Ser1177), Cav-1 (Tyr14), AKT (Ser473), and ERK (T202/Y204)

After overnight serum deprivation in culture medium containing 0.5% FBS or 0.1% FBS for ~5–7 h, agonists were added to cells and incubated for indicated times at 37°C. Inhibitors were added 30 min prior to stimulation. Cells were collected and lysed for Western blotting. After being probed for phosphoryated eNOS (pSer1177), Cav-1 (pTyr14), AKT (pSer473), and ERK (pT202/Y204), the same blots were stripped and reprobed for total eNOS, Cav-1, AKT, and ERK proteins, and actin was probed as a loading control.

Chemiluminescence-based NO measurements

Briefly, HUVECs or HEK293-transfected cells were washed twice with HBSS and incubated with HBSS-Arg (HBSS plus 0.2–0.5 mM L-arginine) for 30 min at 37°C. The cells were then treated with agonists for up to 30 min in HBSS-Arg. NO concentration in the culture media was assessed by measuring NO_2 accumulation as described (Bonini *et al.*, 2002; Chen *et al.*, 2012) using a Sievers NO analyzer (Sievers Instruments). NO release from transfected HEK293 cells was assessed from the NO_2^- level in the media (Bernatchez *et al.*, 2005) and reported as μmol NO_2^-/min per 10^6 cells.

Statistical analysis

Data are expressed as mean ± SEM. Statistical analysis was performed by Student's *t* test or one-way analysis of variance using GraphPad InStat software).

ACKNOWLEDGMENTS

We thank Maricela Castellon for technical assistance. This work was supported by National Institutes of Health Grants P01 HL60678 (R.D.M.) and R01 HL125356 (M.G.B., R.D.M.), American Diabetes Association Grants 1-14-JF-32 and UL1RR029879 (J.M.H.), the UIC Chancellor's Discovery Fund (R.D.M., M.G.B., J.M.H.), and UIC Center for Clinical and Translational Science Institutional Grant UL1TR002003 and Pilot Grant 2017-06 (R.D.M., M.B.G., J.M.H., O.L.).

REFERENCES

Bakhshi FR, Mao M, Shajahan AN, Piegeler T, Chen Z, Chernaya O, Sharma T, Elliott WM, Szulcek R, Bogaard HJ, *et al.* (2013). Nitrosation-dependent caveolin 1 phosphorylation, ubiquitination, and degradation and its association with idiopathic pulmonary arterial hypertension. Pulm Circ 3, 816–830.

Bernatchez PN, Bauer PM, Yu J, Prendergast JS, He P, Sessa WC (2005). Dissecting the molecular control of endothelial NO synthase by caveolin-1 using cell-permeable peptides. Proc Natl Acad Sci USA 102, 761–766.

Bernatchez P, Sharma A, Bauer PM, Marin E, Sessa WC (2011). A noninhibitory mutant of the caveolin-1 scaffolding domain enhances eNOS-derived NO synthesis and vasodilation in mice. J Clin Invest 121, 3747–3755.

Bonini MG, Dull RO, Minshall RD (2014). Caveolin-1 regulation of eNOS function and oxidative stress in the endothelium. In: Systems Biology of Free Radicals and Anti-oxidants, ed. I. Laher, Berlin: Springer-Verlag, 1343–1363.

Bonini MG, Mason RP, Augusto O (2002). The mechanism by which 4-hydroxy-2,2,6,6-tetramethylpiperidene-1-oxyl (tempol) diverts peroxynitrite decomposition from nitrating to nitrosating species. Chem Res Toxicol 15, 506–511.

Chen Z, Bakhshi FR, Shajahan AN, Sharma T, Mao M, Trane A, Bernatchez P, van Nieuw Amerongen GP, Bonini MG, Skidgel RA, *et al.* (2012). Nitric oxide-dependent Src activation and resultant caveolin-1 phosphorylation promote eNOS/caveolin-1 binding and eNOS inhibition. Mol Biol Cell 23, 1388–1398.

Chen Z, Deddish PA, Minshall RD, Becker RP, Erdös EG, Tan F (2006). Human ACE and bradykinin B2 receptors form a complex at the plasma membrane. FASEB J 20, 2261–2270.

Cheng JP, Mendoza-Topaz C, Howard G, Chadwick J, Shvets E, Cowburn AS, Dunmore BJ, Crosby A, Morrell NW, Nichols BJ (2015). Caveolae protect endothelial cells from membrane rupture during increased cardiac output. J Cell Biol 211, 53–61.

Cheng JP, Nichols BJ (2016). Caveolae: one function or many? Trends Cell Biol 26, 177–189.

Cohen AW, Park DS, Woodman SE, Williams TM, Chandra M, Shirani J, Pereira de Souza A, Kitsis RN, Russell RG, Weiss LM, *et al.* (2003). Caveolin-1 null mice develop cardiac hypertrophy with hyperactivation of p42/44 MAP kinase in cardiac fibroblasts. Am J Physiol Cell Physiol 284, C457–C474.

Couet J, Li S, Okamoto T, Ikezu T, Lisanti MP (1997). Identification of peptide and protein ligands for the caveolin-scaffolding domain. Implications for the interaction of caveolin with caveolae-associated proteins. J Biol Chem 272, 6525–6533.

Drab M, Verkade P, Elger M, Kasper M, Lohn M, Lauterbach B, Menne J, Lindschau C, Mende F, Luft FC, *et al.* (2001). Loss of caveolae, vascular dysfunction, and pulmonary defects in caveolin-1 gene-disrupted mice. Science 293, 2449–2452.

Dröge W (2002). Free radicals in the physiological control of cell function. Physiol Rev 82, 47–95.

Dudzinski DM, Igarashi J, Greif D, Michel T (2006). The regulation and pharmacology of endothelial nitric oxide synthase. Annu Rev Pharmacol Toxicol 46, 235–276.

Durán WN, Beuve AV, Sánchez FA (2013). Nitric oxide, S-nitrosation, and endothelial permeability. IUBMB Life 65, 819–826.

Fernandez I, Ying Y, Albanesi J, Anderson RG (2002). Mechanism of caveolin filament assembly. Proc Natl Acad Sci USA 99, 11193–11198.

Fernández-Hernando C, Yu J, Suárez Y, Rahner C, Dávalos A, Lasunción MA, Sessa WC (2009). Genetic evidence supporting a critical role of endothelial caveolin-1 during the progression of atherosclerosis. Cell Metab 10, 48–54.

Frank PG, Pavlides S, Cheung MW, Daumer K, Lisanti MP (2008). Role of caveolin-1 in the regulation of lipoprotein metabolism. Am J Physiol Cell Physiol 295, C242–C248.

Frank PG, Woodman SE, Park DS, Lisanti MP (2003). Caveolin, caveolae, and endothelial cell function. Arterioscler Thromb Vasc Biol 23, 1161–1168.

Fulton D, Babbitt R, Zoellner S, Fontana J, Acevedo L, McCabe TJ, Iwakiri Y, Sessa WC (2004). Targeting of endothelial nitric-oxide synthase to the cytoplasmic face of the Golgi complex or plasma membrane regulates Akt- versus calcium-dependent mechanisms for nitric oxide release. J Biol Chem 279, 30349–30357.

Fulton D, Gratton JP, McCabe TJ, Fontana J, Fujio Y, Walsh K, Franke TF, Papapetropoulos A, Sessa WC (1999). Regulation of endothelium-derived nitric oxide production by the protein kinase Akt. Nature 399, 597–601.

Godo S, Sawada A, Saito H, Ikeda S, Enkhjargal B, Suzuki K, Tanaka S, Shimokawa H (2016). Disruption of physiological balance between nitric oxide and endothelium-dependent hyperpolarization impairs cardiovascular homeostasis in mice. Arterioscler Thromb Vasc Biol 36, 97–107.

Govers R, Bevers L, de Bree P, Rabelink TJ (2002). Endothelial nitric oxide synthase activity is linked to its presence at cell–cell contacts. Biochem J 361(Pt 2), 193–201.

Han B, Tiwari A, Kenworthy AK (2015). Tagging strategies strongly affect the fate of overexpressed caveolin-1. Traffic 16, 417–438.

Hayer A, Stoeber M, Ritz D, Engel S, Meyer HH, Helenius A (2010). Caveolin-1 is ubiquitinated and targeted to intralumenal vesicles in endolysosomes for degradation. J Cell Biol 191, 615–629.

Head BP, Peart JN, Panneerselvam M, Yokoyama T, Pearn ML, Niesman IR, Bonds JA, Schilling JM, Miyanohara A, Headrick J, *et al.* (2010). Loss of caveolin-1 accelerates neurodegeneration and aging. PLoS One 5, e15697.

Hu G, Schwartz DE, Shajahan AN, Visintine DJ, Salem MR, Crystal GJ, Albrecht RF, Vogel SM, Minshall RD (2006). Isoflurane, but not sevoflurane, increases transendothelial albumin permeability in the isolated rat lung: role for enhanced phosphorylation of caveolin-1. Anesthesiology 104, 777–785.

Hu G, Vogel SM, Schwartz DE, Malik AB, Minshall RD (2008). Intercellular adhesion molecule-1-dependent neutrophil adhesion to endothelial

cells induces caveolae-mediated pulmonary vascular hyperpermeability. Circ Res 102, e120–e131.
Iwakiri Y (2011). S-nitrosylation of proteins: a new insight into endothelial cell function regulated by eNOS-devived NO. Nitric Oxide 25, 95–101.
Jaffrey SR, Snyder SH (2001). The biotin switch method for the detection of S-nitrosylated proteins. Sci STKE 2001, pl1.
Jia G, Sowers JR (2015). Caveolin-1 in cardiovascular disease: a double-edged sword. Diabetes 64, 3645–3647. Arterioscler Thromb Vasc Biol 36, 97–107.
Ju H, Zou R, Venema VJ, Venema RC (1997). Direct interaction of endothelial nitric-oxide synthase and caveolin-1 inhibits synthase activity. J Biol Chem 272, 18522–18525.
Li H, Witte K, August M, Brausch I, Gödtel-Armbrust U, Habermeier A, Closs EI, Oelze M, Münzel T, Förstermann U (2006). Reversal of endothelial nitric oxide synthase uncoupling and up-regulation of endothelial nitric oxide synthase expression lowers blood pressure in hypertensive rats. J Am Coll Cardiol 47, 2536–2544.
Li L, Ren CH, Tahir SA, Ren C, Thompson TC (2003). Caveolin-1 maintains activated Akt in prostate cancer cells through scaffolding domain binding site interactions with and inhibition of serine/threonine protein phosphatases PP1 and PP2A. Mol Cell Biol 23, 9389–9404.
Liu G, Place AT, Chen Z, Brovkovych VM, Vogel SM, Muller WA, Skidgel RA, Malik AB, Minshall RD (2012). ICAM-1-activated Src and eNOS signaling increase endothelial cell surface PECAM-1 adhesivity and neutrophil transmigration. Blood 120, 1942–1952.
Liu J, García-Cardeña G, Sessa WC (1996). Palmitoylation of endothelial nitric oxide synthase is necessary for optimal stimulated release of nitric oxide: implications for caveolae localization. Biochemistry 35, 13277–13281.
Lundberg JO, Gladwin MT, Weitzberg E (2015). Strategies to increase nitric oxide signaling in cardiovascular disease. Nat Rev Drug Discov 14, 623–641.
Mahmoud AM, Szczurek MR, Blackburn BK, Mey JT, Chen Z, Robinson AT, Bian JT, Unterman TG, Minshall RD, Brown MD, *et al*. (2016). Hyperinsulinemia augments endothelin-1 protein expression and impairs vasodilation of human skeletal muscle arterioles. Physiol Rep 4, e12895.
Maniatis NA, Brovkovych V, Allen SE, John TA, Shajahan AN, Tiruppathi C, Vogel SM, Skidgel RA, Malik AB, Minshall RD (2006). Novel mechanism of endothelial nitric oxide synthase activation mediated by caveolae internalization in endothelial cells. Circ Res 99, 870–877.
Maniatis NA, Shinin V, Schraufnagel DE, Okada S, Vogel SM, Malik AB, Minshall RD (2008). Increased pulmonary vascular resistance and defective pulmonary artery filling in caveolin-1-/- mice. Am J Physiol Lung Cell Mol Physiol 294, L865–L873.
Mao M, Varadarajan S, Fukai T, Bakhshi FR, Chernaya O, Dudley SC Jr, Minshall RD, Bonini MG (2014). Nitroglycerin tolerance in caveolin-1 deficient mice. PLoS One 9, e104101.
Mey JT, Blackburn BK, Miranda ER, Chaves AB, Briller J, Bonini MG, Haus JM (2018). Dicarbonyl stress and glyoxalase enzymatic system regulation in human skeletal muscle. Am J Physiol Regul Integr Comp Physiol 314, R181–R190.
Michel JB, Feron O, Sacks D, Michel T (1997). Reciprocal regulation of endothelial nitric-oxide synthase by Ca2+-calmodulin and caveolin. J Biol Chem 272, 15583–15586.
Michel JB, Michel T (1997). The role of palmitoyl-protein thioesterase in the palmitoylation of endothelial nitric oxide synthase. FEBS Lett 405, 356–362.
Minshall RD, Tiruppathi C, Vogel SM, Niles WD, Gilchrist A, Hamm HE, Malik AB (2000). Endothelial cell-surface gp60 activates vesicle formation and trafficking via G(i)-coupled Src kinase signaling pathway. J Cell Biol 150, 1057–1070.
Monier S, Dietzen DJ, Hastings WR, Lublin DM, Kurzchalia TV (1996). Oligomerization of VIP21-caveolin in vitro is stabilized by long chain fatty acylation or cholesterol. FEBS Lett 388, 143–149.
Moroi M, Zhang L, Yasuda T, Virmani R, Gold HK, Fishman MC, Huang P L (1998). Interaction of genetic deficiency of endothelial nitric oxide, gender, and pregnancy in vascular response to injury in mice. J Clin Invest 101, 1225–1232.
Murata T, Lin MI, Huang Y, Yu J, Bauer PM, Giordano FJ, Sessa WC (2007). Reexpression of caveolin-1 in endothelium rescues the vascular, cardiac, and pulmonary defects in global caveolin-1 knockout mice. J Exp Med 204, 2373–2382.
Oliveira SDS, Castellon M, Chen J, Bonini MG, Gu X, Elliott MH, Machado RF, Minshall RD (2017). Inflammation-induced caveolin-1 and BMPRII depletion promotes endothelial dysfunction and TGF-β-driven pulmonary vascular remodeling. Am J Physiol Lung Cell Mol Physiol 312, L760–L771.
Oritz PA, Garvin JL (2003). Trafficking and activation of eNOS in epithelial cells. Acta Physiol Scand 179, 107–114.
Orlichenko L, Weller SG, Cao H, Krueger EW, Awoniyi M, Beznoussenko G, Buccione R, McNiven MA (2009). Caveolae mediate growth factor-induced disassembly of adherens junctions to support tumor cell dissociation. Mol Biol Cell 20, 4140–4152.
Parton RG, del Pozo MA (2013). Caveolae as plasma membrane sensors, protectors and organizers. Nat Rev Mol Cell Biol 14, 98–112.
Parton RG, Simons K (2007). The multiple faces of caveolae. Nat Rev Mol Cell Biol 8, 185–194.
Pavlides S, Gutierrez-Pajares JL, Iturrieta J, Lisanti MP, Frank PG (2014). Endothelial caveolin-1 plays a major role in the development of atherosclerosis. Cell Tissue Res 356, 147–157.
Prabhakar P, Cheng V, Michel T (2000). A chimeric transmembrane domain directs endothelial nitric-oxide synthase palmitoylation and targeting to plasmalemmal caveolae. J Biol Chem 275, 19416–19421.
Qian J, Fulton D (2013). Post-translational regulation of endothelial nitric oxide synthase in vascular endothelium. Front Physiol 4, 347.
Razani B, Engelman JA, Wang XB, Schubert W, Zhang XL, Marks CB, Macaluso F, Russell RG, Li M, Pestell RG, *et al*. (2001). Caveolin-1 null mice are viable but show evidence of hyperproliferative and vascular abnormalities. J Biol Chem 276, 38121–38138.
Robinson LJ, Michel T (1995). Mutagenesis of palmitoylation sites in endothelial nitric oxide synthase identifies a novel motif for dual acylation and subcellular targeting. Proc Natl Acad Sci USA 92, 11776–11780.
Sánchez FA, Kim DD, Durán RG, Meininger CJ, Durán WN (2008). Internalization of eNOS via caveolae regulates PAF-induced inflammatory hyperpermeability to macromolecules. Am J Physiol Heart Circ Physiol 295, H1642–H1648.
Sargiacomo M, Scherer PE, Tang Z, Kübler E, Song KS, Sanders MC, Lisanti MP (1995). Oligomeric structure of caveolin: implications for caveolae membrane organization. Proc Natl Acad Sci USA 92, 9407–9411.
Scherer PE, Lewis RY, Volonte D, Engelman JA, Galbiati F, Couet J, Kohtz DS, van Donselaar E, Peters P, Lisanti MP (1997). Cell-type and tissue-specific expression of caveolin-2. Caveolins 1 and 2 co-localize and form a stable hetero-oligomeric complex in vivo. J Biol Chem 272, 29337–29346.
Schubert W, Frank PG, Razani B, Park DS, Chow CW, Lisanti MP (2001). Caveolae-deficient endothelial cells show defects in the uptake and transport of albumin in vivo. J Biol Chem 276, 48619–48622.
Scotland RS, Morales-Ruiz M, Chen Y, Yu J, Rudic RD, Fulton D, Gratton JP, Sessa WC (2002). Functional reconstitution of endothelial nitric oxide synthase reveals the importance of serine 1179 in endothelium-dependent vasomotion. Circ Res 90, 904–910.
Sears CE, Bryant SM, Ashley EA, Lygate CA, Rakovic S, Wallis HL, Neubauer S, Terrar DA, Casadei B (2003). Cardiac neuronal nitric oxide synthase isoform regulates myocardial contraction and calcium handling. Circ Res 92, e52–e59.
Shajahan AN, Tiruppathi C, Smrcka AV, Malik AB, Minshall RD (2004). Gbetagamma activation of Src induces caveolae-mediated endocytosis in endothelial cells. J Biol Chem 279, 48055–48062.
Shaul PW, Smart EJ, Robinson LJ, German Z, Yuhanna IS, Ying Y, Anderson RG, Michel T (1996). Acylation targets emdothelial nitric-oxide synthase to plasmalemmal caveolae. J Biol Chem 271, 6518–6522.
Shen BQ, Lee DY, Zioncheck TF (1999). Vascular endothelial growth factor governs endothelial nitric-oxide synthase expression via a KDR/Flk-1 receptor and a protein kinase C signaling pathway. J Biol Chem 274, 33057–33063.
Shvets E, Ludwig A, Nichols BJ (2014). News from the caves: update on the structure and function of caveolae. Curr Opin Cell Biol 29, 99–106.
Song KS, Tang Z, Li S, Lisanti MP (1997). Mutational analysis of the properties of caveolin-1. A novel role for the C-terminal domain in mediating homo-typic caveolin-caveolin interactions. J Biol Chem 272, 4398–4403.
Sowa G (2012). Caveolae, caveolins, cavins, and endothelial cell function: new insights. Front Physiol 2, 120.
Sun Y, Hu G, Zhang X, Minshall RD (2009). Phosphorylation of caveolin-1 regulates oxidant-induced pulmonary vascular permeability via paracellular and transcellular pathways. Circ Res 105, 676–685.
Sverdlov M, Shinin V, Place AT, Castellon M, Minshall RD (2009). Filamin A regulates caveolae internalization and trafficking in endothelial cells. Mol Biol Cell 20, 4531–4540.
Thomas DD, Liu X, Kantrow SP, Lancaster JR Jr (2001). The biological lifetime of nitric oxide: implications for the perivascular dynamics of NO and O_2. Proc Natl Acad Sci USA 98, 355–360.

Tiruppathi C, Song W, Bergenfeldt M, Sass P, Malik AB (1997). Gp60 activation mediates albumin transcytosis in endothelial cells by tyrosine kinase-dependent pathway. J Biol Chem 272, 25968–25975.
Trane AE, Pavlov D, Sharma A, Saqib U, Lau K, van Petegem F, Minshall RD, Roman LJ, Bernatchez PN (2014). Deciphering the binding of caveolin-1 to client protein endothelial nitric-oxide synthase (eNOS): scaffolding subdomain identification, interaction modeling, and biological significance. J Biol Chem 289, 13273–13283.
Wang H, Wang AX, Aylor K, Barrett EJ (2015). Caveolin-1 phosphorylation regulates vascular endothelial insulin uptake and is impaired by insulin resistance in rats. Diabetologia 58, 1344–1353.
Wang H, Wang AX, Barrett EJ (2011). Caveolin-1 is required for vascular endothelial insulin uptake. Am J Physiol Endocrinol Metab 300, E134–E144.
Wang H, Wang AX, Liu Z, Chai W, Barrett EJ (2009). The trafficking/interaction of eNOS and caveolin-1 induced by insulin modulates endothelial nitric oxide production. Mol Endocrinol 23, 1613–1623.
Williamson DL, Dungan CM, Mahmoud AM, Mey JT, Blackburn BK, Haus JM (2015). Aberrant REDD1-mTORC1 responses to insulin in skeletal muscle from Type 2 diabetics. Am J Physiol Regul Integr Comp Physiol 309, R855–R863.
Yue L, Bian JT, Grizelj I, Cavka A, Phillips SA, Makino A, Mazzone T (2012). Apolipoprotein E enhances endothelial-NO production by modulating caveolin 1 interaction with endothelial NO synthase. Hypertension 60, 1040–1046.
Zhang Q, Church JE, Jagnandan D, Catravas JD, Sessa WC, Fulton D (2006). Functional relevance of Golgi- and plasma membrane-localized endothelial NO synthase in reconstituted endothelial cells. Arterioscler Thromb Vasc Biol 26, 1015–1021.
Zhao Y, Vanhoutte PM, Leung SW (2015). Vascular nitric oxide: beyond eNOS. J Pharmacol Sci 129, 83–94.
Zhao YY, Liu Y, Stan RV, Fan L, Gu Y, Dalton N, Chu PH, Peterson K, Ross J Jr, Chien KR (2002). Defects in caveolin-1 cause dilated cardiomyopathy and pulmonary hypertension in knockout mice. Proc Natl Acad Sci USA 99, 11375–11380.
Zimnicka AM, Husain YS, Shajahan AN, Sverdlov M, Chaga O, Chen Z, Toth PT, Klomp J, Karginov AV, Tiruppathi C, *et al*. (2016). Src-dependent phosphorylation of caveolin-1 Tyr-14 promotes swelling and release of caveolae. Mol Biol Cell 27, 2090–2106.